

Electrocatalytic Oxidation of Ethanol on Platinum Electrode Decorated with Nd-Fe-Mo Hybrid-metallic Cyano-Bridged Mixing Coordination Polymer in Weak Acidic Medium

Yongjun Ma^{1,2}, Yongling Du¹, Weichun Ye¹, Biquan Su¹, Meixia Yang¹ and Chunming Wang^{1,*}

¹ Department of Chemistry, Lanzhou University, Lanzhou 730000, China.

² College of Chemistry & Chemical Engineering, Northwest Normal University, Lanzhou 730070, China.

*E-mail: wangcm@lzu.edu.cn

Received: 22 December 2011 / Accepted: 31 January 2012 / Published: 1 March 2012

In the present work, a novel Nd-Fe-Mo hybrid-metallic cyano-bridged mixing coordination polymer decorated platinum electrode is successfully prepared by electrodeposition. There are the excellent synergistic catalytic activity and the remarkable CO-poisoning tolerance on the decorated polycrystalline platinum surface for ethanol electrooxidation. In weak acidic medium, the electrocatalytic oxidation of ethanol is studied in detail by using cyclic voltammetry and chronoamperometry. Here, we observe the presence of five distinct current peaks related to the ethanol electrooxidation process and primarily reveal their electrochemical nature. Besides, through voltammetric data analysis, the kinetic behavior of peak 4 is considered as a diffusion-controlled electrochemical process and therefore the nature of peak 4 is reasonably attributed to the more plentiful production of acetaldehyde via a one-step concerted dehydrogenation pathway of ethanol. These results imply that the electrooxidation of ethanol possibly follows different dehydrogenation pathways on a decorated platinum electrode. In addition, according to Arrhenius plots, the apparent activation energies (E_a) of ethanol oxidation are calculated as 22.78kJ/mol for peak 1, 18.85kJ/mol for peak 2 and 29.38kJ/mol for peak 4, respectively. Based on the particular experimental evidences, a new dehydrogenation model is proposed to the preliminary interpretation of the mechanism of ethanol electrooxidation.

Keywords: Ethanol; Electrocatalytic oxidation; Cyano-bridged coordination; Modified electrode

1. INTRODUCTION

With the development of fuel cell technology, the direct ethanol fuel cell (DEFC) has attracted more and more attention [1-3]. As a fuel that promises the development of a commercial fuel cell, ethanol receives considerable interest because of its low toxicity and economic feasibility due to

expedient large-scale production through the fermentation of biomass. Furthermore, if the fuel ethanol could be completely converted to carbon dioxide at the anode of a fuel cell that is coupled to the reduction reaction of molecular oxygen at the fuel cell's cathode, it would possess of a high theoretical energy density of 8.0 kWh/kg [2, 4]. However, under acidic conditions, the oxidation of ethanol in a conventional fuel cell actually yields acetaldehyde and acetic acid as its main products as well as a small proportional amount of carbon dioxide, and the production of those incompletely oxidized substances significantly reduces the fuel cell's energy output efficiency [5-9]. Moreover, some toxic intermediates, especially CO that produced in the ethanol oxidation process will be adsorbed strongly onto the electrode surface and poison the anode catalyst. Therefore, how to clarify the ethanol oxidation pathways related to production distribution and how to exploit a new method of preparing a CO-tolerant anode catalyst have become two important research issues in the commercialization of DEFCs [5, 8-11].

Currently, the best efficient catalysts for the electrocatalytic oxidation of ethanol in acidic medium are still Pt-based metal catalysts [10-14], Pt-oxide catalysts [15-18] and other platinum/carbon materials composite catalysts [3, 19-21]. Since the activity of anode catalysts is affected by the elemental composition of catalysts' interfaces, the use of other compounds for the modification of platinum substrates will help to improve the performance of platinum catalysts and even change the distribution of ethanol oxidation products [22-25]. By means of the superficial modification of other additive elements, which is the so-called decoration of platinum electrodes, the cooperative catalytic effect resulted from the redesign of the environment around Pt-atom active centers will promotes the kinetics of ethanol oxidation remarkably [26-30]. In various modified compounds, the materials containing rare-earth elements have been considered to be the most effective and cost-efficient materials for improving the catalytic activity [31-35]. It has been reported that the rare-earth components of catalysts can take effect by weakening the affection of the poisoning intermediates during aliphatic alcohol electrooxidation [31, 35].

Metal hexacyanoferrates (MHCFs), such as the Prussian blue and its analogues (PBAs), have previously been exploited as battery electrode materials in secondary cells; however, their applications as the anodic catalyst of fuel cells are sparsely reported in the literatures [36-39]. Fortunately, as promising catalytic materials for aliphatic alcohol electrooxidation, their specific electrocatalytic activity when decorated on the glass carbon electrodes in ruthenium-iron cyano-bridged complex patterns has been recognized to a certain extent [40]. In the past few decades, a series of Ln-Fe cyano-bridged 3d-4f complexes, with or without an organic ligand in their molecular structure, have been extensively developed mainly due to their extraordinary molecular magnetic character rather than their catalytic activity [41-44], while a platinum electrode decorated with the hybrid-metallic cyano-bridged d-f complexes exhibit excellent electrocatalytic activity towards the electrooxidation of methanol and formic acid in our previous works [45-46].

A promising objective of this study is the construction of a novel hybrid trimetallic cyano-bridged mixing coordination polymer (Nd-Fe-Mo) due to its potential applications as a DEFC's anode catalyst component, in which phthalate and molybdate anions are the ligands of the neodymium ion and ferricyanide anions act as bridged-bond building-blocks molecules. The new hybrid-metallic cyano-bridged d-f compounds form a desirable topological network with respect to neodymium, iron

and molybdenum. Furthermore, in weak acidic medium, the voltammetric behaviors of ethanol electrooxidation on the Nd-Fe-Mo decorated platinum electrode are studied in detail. A synergistic catalytic effect and an excellent voltammetric characteristic for ethanol electrooxidation reaction are obtained in the present electrode. With the Nd-Fe-Mo decorated platinum electrode, the information concerning the voltammetric behaviors of ethanol electrooxidation can be perceived better and more accurately, which might provide further insight into the nature of ethanol oxidation reaction (EOR). Based on the experimental results, a new mechanistic model is inferred to interpret the ethanol oxidation process.

2. EXPERIMENTAL

2.1. Chemicals

Neodymium oxide (99.99% high purity reagents) and Ethanol (A.R.) were purchased from Sino-pharm. Group Co., China. 3,4-dihydroxyphenethylamine hydrochloride (dopamine) was purchased from Sigma-Aldrich and concentrated sulfuric acid (98%, G.R.) was obtained from Beijing Chemical Works, Beijing, China. Potassium ferricyanide (A.R.) was purified by recrystallization in pure water. All chemicals were of analytical grade except for special statement and were used without further treatment. Doubly distilled water and high-purity argon gas were used throughout the experiments.

2.2. Preparation of the Nd-Fe-Mo decorated platinum disc electrode.

A bare platinum disc electrode was primarily polished using emery paper (1200 mesh number) and further polished with two kinds of aqueous slurry of alumina powder (Al_2O_3 , 0.05 μm and 0.3 μm) to a mirror plane. Then, it was ultrasonically cleaned sequentially in KOH (5M), HNO_3 (1:1) and 50% (v/v) acetone (1min for each). After thoroughly rinsing, the Pt electrode was immersed into the electroplating solution and five potential segments ranging from 0.55 to -0.31 V (vs. SCE) were swept at a scan rate of 83mVs^{-1} to obtain the suitable sedimentary amounts of the Nd-Fe-Mo materials. As the last decorated procedure, the Nd-Fe-Mo decorated electrode was also swept from 0.50 to -0.60 V (vs. SCE) by 6 cycles in a electrolyte containing 2.5×10^{-3} M dopamine + 0.06 M PBS solution (pH 7.0) to obtain a protecting layer of polydopamine on the decorated Nd-Fe-Mo deposits. The production of polydopamine had no effect on the ethanol electrooxidation process, but would help to increase adhesiveness of the Nd-Fe-Mo decoration deposits on the platinum electrode surface in order to maintain the catalytic activity over a period of least two weeks. Before proceeding with the subsequent electrochemical experiments, the decorated electrode had to be swept again to achieve its steady cyclic voltammograms in 0.2 M chloroacetic acid/chloroacetate buffer solution by cycling from 0 to 1.10 V potential regions at a scan rate of 100mVs^{-1} . The electroplating solution for manufacturing the Nd-Fe-Mo decorated electrode was made by combining two initial aqueous solutions in which solution (a) contained 22.5 μmol neodymium nitrate, 1.88 μmol potassium hydrogen phthalate and 5.63 μmol ammonium molybdate, and solution (b) contained 0.63 μmol ferric nitrate, 2.50 μmol potassium

ferricyanide and 5.63 mmol potassium nitrate. Solution (a) and (b) were slowly mixed and diluted to 25.0mL with aqueous solutions containing appropriate amounts of Triton-X100 and chloroacetic acid/chloroacetate buffer solution. But it was noticeable that the ratio between the amounts of each reagent must be very precise and pH value of the deposition solution was adjusted to 1.83 with a diluting HNO_3 solution for electrodeposition procedure.

2.3. Instrumentation and Measurements.

A field-emission scanning electron microscopy (JSM-6701, JEOL, Japan), FTS3000 infrared spectrometer (DIGILAB Corp., U.S.A), RFS-100 Raman spectrometer (Bruker, Germany) and D/MAX-MC X-ray diffractometer (Rigaku Corp., Japan) were used to character the Nd-Fe-Mo decoration materials.

The electrochemical properties of ethanol oxidation were studied using a CHI760B electrochemical workstation (CHI Instruments, U.S.A.) in a conventional three-electrode cell, which was made up of a decorated or bare polycrystalline platinum disk (purity: 99.99%, diameter: 2 mm, Gaoss Union, Ltd., Wuhan, China.) as the working electrode, a platinum foil (geometric area: 1cm^2) as the auxiliary electrode and mercury/mercurous sulfate electrode ($\text{Hg}/\text{Hg}_2\text{SO}_4$) as the reference electrode. All potentials in this experiment were measured against the $\text{Hg}/\text{Hg}_2\text{SO}_4$ electrode, while the current density of the voltammetric peak was normalized to the geometric area of the platinum substrate. In the electrochemical experiments, the quiet time during the initial scan potential was set to 14s and the potential scanning range was from -0.5 V to 1.2 V. The other experimental conditions were clearly indicated in the caption of Figure 3 unless the changes in electrolyte composition were explicitly expressed otherwise. The voltammetric tests were generally performed within the temperature range $25\pm 1^\circ\text{C}$, which was adjusted using a thermostat.

2.4. Characterization of the Nd-Fe-Mo decorated platinum disc electrode.

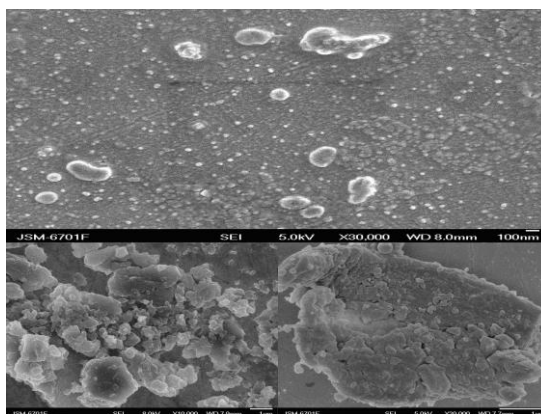


Figure 1. SEM image of Nd-Fe-Mo cyano-bridged mixing coordination polymer materials on the decorated platinum surface. Bottom inset: high-resolution SEM micrograph for the indicated the biggish pieces of Nd-Fe-Mo deposits.

As shown in Figure 1, the SEM micrograph of the Nd-Fe-Mo decorated platinum electrode is obtained by using the field-emission scanning electron microscopy. The decorated Nd-Fe-Mo materials on platinum substrate appeared as a granular aggregation structure and its biggish pieces in shape show laminated crystalloid texture, whereas the Nd-Fe-Mo decoration does not coat the platinum electrode surface entirely.

The electrochemical behavior of Nd-Fe-Mo decorated platinum electrode and glass carbon electrode are investigated in a 0.2 M chloroacetic acid/chloroacetate buffer solution. As can be seen from Figure 2, three pairs of well-defined redox peaks (1a/1b, 2a/2b and 3a/3b) with their formal potential about 0.00V, 0.12V and 0.79V confirm the presence of Nd-Fe-Mo polymer decorated materials. Obviously, the Nd-Fe-Mo hybrid-metallic cyano-bridged mixing coordination polymer shows particular voltammetric properties that are distinguished from common cyano-bridged complexes such as neodymium hexacyanoferrate and molybdenum hexacyanoferrate [47-48]. However, for the electrocatalytic oxidation of ethanol, the Nd-Fe-Mo materials decorated on platinum electrode but not on glass carbon electrode can exhibit the improvement of the catalytic performance. Similar to the action of metal ruthenium in Pt-Ru alloy for the ethanol oxidation [49], the action of Nd-Fe-Mo polymer on decorated electrode surface almost come from the synergistic catalytic action for EOR.

Furthermore, compared curve (b) with curve (d) in Figure 2, it is observed that the voltammetric peaks attributed to the decoration materials themselves appear faintly on a decorated platinum electrode rather than on a decorated glass carbon electrode. Hence, in 0.5 M sulfuric acid solution, it is still showed distinctly that the typical voltammetric peaks of adsorption/desorption hydrogen does before and after Nd-Fe-Mo decoration on the platinum electrode.

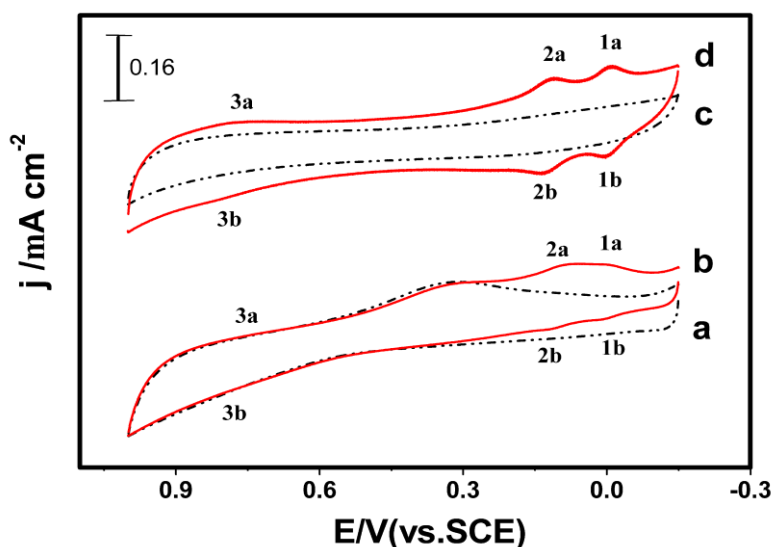
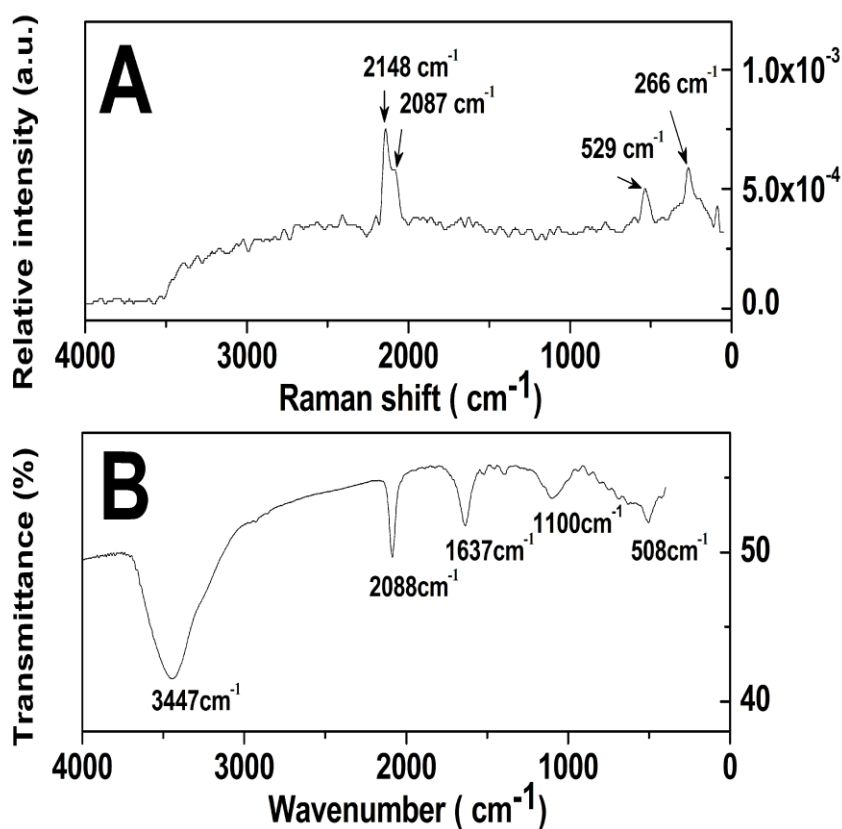


Figure 2. Cyclic voltammograms of a platinum electrode (a, b) and glass carbon electrode (c, d) are obtained in 0.2 M chloroacetic acid/chloroacetate buffer solution corresponding to the absence of decoration (a, c) and the presence of decoration (b, d). Scan rate is of 100mVs^{-1} . The cyclic scan number of electrodeposition is 10 in decorated procedure.

By comparing with the CV peak integration area of both an Nd-Fe-Mo decorated platinum electrode and a bare platinum electrode between ca. -0.47 V and -0.60 V (vs. Hg/Hg₂SO₄), the surface coverage ratio of the Nd-Fe-Mo decoration materials on the platinum electrode surface is then handily estimated to be 47.6%. Thus, if the total coverage on platinum electrode is too low, the benefit of catalytic improvement is not observed; but if it is too high, a decorated Nd-Fe-Mo materials may occupy too much of the effective catalytic surface of the platinum electrode and produce a poor catalytic effect. Given this, only under the appropriate coverage, are the best synergistic catalytic effects achieved. In fact, the optimal coverage of the Nd-Fe-Mo polymer coated on a platinum electrode surface can be acquired by controlling the voltammetric parameters of the electrodeposition process.

In addition, the molecular structure information of the decorated materials is tested using FT-IR and FT-Raman spectra. As seen in Figure 3, there are the Raman peaks around 2148 cm⁻¹ and a strong infrared absorption band of 2088 cm⁻¹ for Nd-Fe-Mo polymer deposits, which are assigned to the characteristic of C-N bond's stretching band of the d-f cyano-bridged complexes [47, 50-51]. Moreover, the synthesized coordination polymer is also examined by XRD measurements. Although the diffraction peaks at $2\theta = 17.5^\circ, 24.6^\circ, 35.2^\circ, 39.6^\circ, 50.7^\circ, 54.0^\circ, 57.4^\circ$ are resemble to diffraction peaks of the pure face-centered-cubic phase of the Prussian blue analogue [52], an exceptional diffraction peak at $2\theta = 26.7^\circ$ implies the existence of a particularity due to a d-f heterometallic framework structure [44,47,51]. The spectral data mentioned above confirm the existence of a new class of Nd-Fe-Mo cyano-bridged mixing coordination polymer.



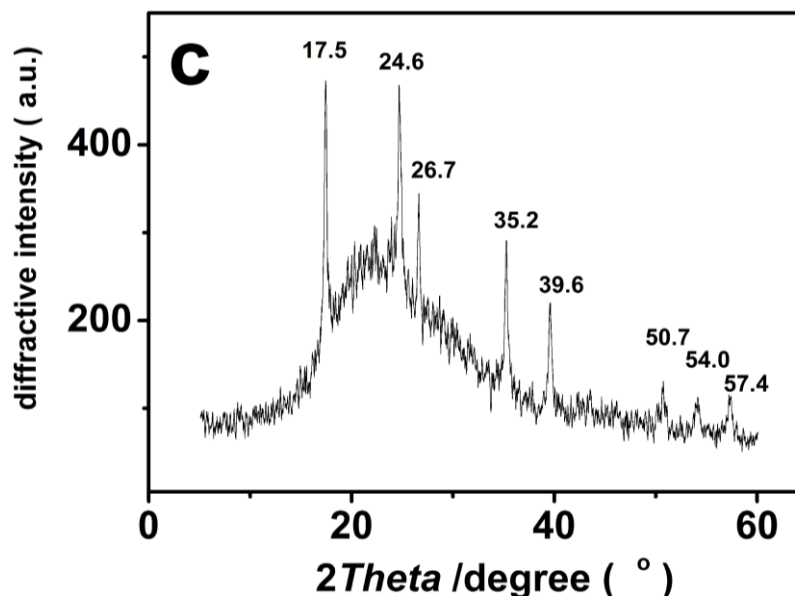


Figure 3. FT-IR spectroscopy (A), FT-Raman spectroscopy (B) and XRD patterns (C) of the Nd-Fe-Mo cyano-bridged mixing coordination polymer materials. The Nd:YAG laser has the output power of 100 mW for FT-Raman analysis and data are collected at 4 cm^{-1} resolution with 100 scans. The X-ray gun was operated at 40 kV and 30 mA with nickel-filtered Cu/ $K\alpha$ radiation and scan rate was of 4 degrees/min (2-theta degree).

3. RESULTS AND DISCUSSION

3.1. Catalytic Activation of Ethanol Oxidation at Decorated Platinum Electrodes.

As a well-known fact, several cyclic scans must be performed in a testing solution before the recordable voltammograms can be obtained. It is shown in Figure 4 that exhibits the variation of the cyclic voltammograms of ethanol during multiple scanning. The peak current of ethanol oxidation gradually increased to a considerable value during successive potential scanning at both the bare platinum electrodes and the decorated platinum electrodes. Compared voltammograms (a) with (b) in Figure 4, it is observed that the accomplishment of catalytic activation is more rapid on the Nd-Fe-Mo decorated platinum electrode than on a bare platinum electrode. After completing the catalytic activation (Figure 4, see inset), the peak current density of EOR increase about 58% for peak 1 and 36% for peak 2 on the Nd-Fe-Mo decorated electrode compared with that on the bare platinum electrode, respectively. In practice, even though the decoration reduces the net platinum surface area, the increases of oxidation peak current are still remarkable. The fact suggests that the promotion of electrocatalytic activity for ethanol electrooxidation should be entirely attributed to the synergistic catalytic effect between the Nd-Fe-Mo materials and the platinum active sites.

Simultaneously, it is also observed that the peak potentials of peak 1, peak 4 and peak 5 synchronously shifted to more positive values, while the potential value of peak 2 is comparatively stable during the successive potential scanning. It implies that there is an intrinsic interaction among peak 1, peak 4 and peak 5. Surprisingly, if the activated electrode is replaced into the cell containing

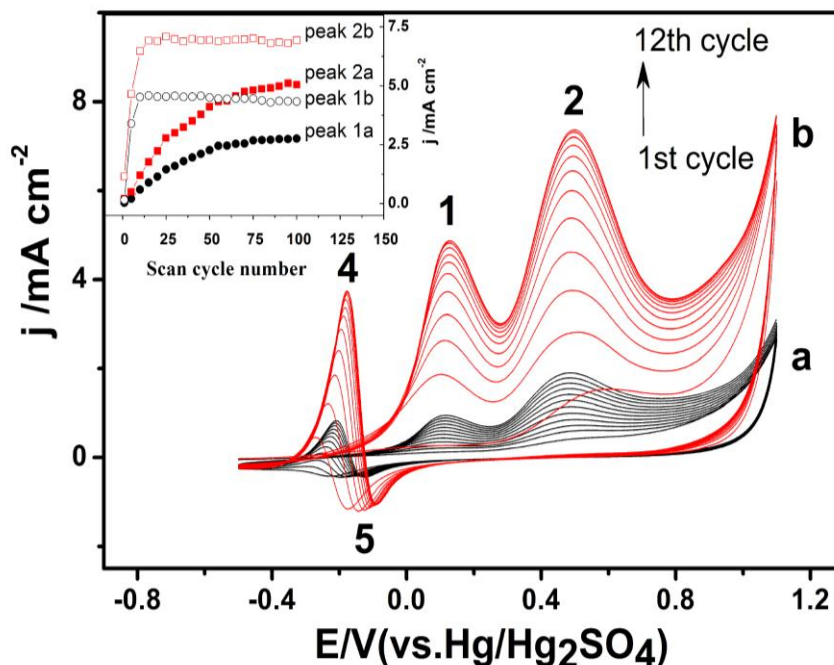


Figure 4. Successive cyclic voltammograms of 0.25 M ethanol at a bare platinum electrode (a) and the Nd-Fe-Mo decorated electrode (b). Supporting electrolyte is composed of 0.45 M sodium sulfate + 1.0×10^{-3} M sulfuric acid. Inset curves show the relationship between the forward peak current of ethanol oxidation and the scan cyclic number. Scan rate is 100 mVs^{-1} . Electrode area is 0.0314 cm^2 .

ethanol solution after thoroughly rinsed with doubly distilled water, its catalytic activation for ethanol oxidation would initially reduced and then reconverted to its activated state with the increase in the cyclic scanning number. In this way, the catalytic activity of the electrode for ethanol oxidation would be promoted by an unrecognized reactive intermediate that may be produced during cyclic voltammetric scanning, and the process of ethanol oxidation on the decorated platinum electrode would be an autocatalytic process. Thus, before proceeding with the study of electrochemical behavior for EOR, the working electrodes have to be activated in 0.25 M EtOH + 1.0×10^{-3} M sulfuric acid + 0.45 M sodium sulfate solution by cycling 100 repetitions for the decorated electrode and by cycling 500 repetitions for the bare electrode, respectively. Significantly, in view of the fact that the behavior of catalyst's activation for the electrooxidation of methanol, formaldehyde and formic acid are their commonness on the Nd-Fe-Mo decorated platinum electrode, the unrecognized reactive intermediate should be considered to be a common byproduct that produces in electrooxidation process of these small organic molecules.

3.2. Effects of pH and SO_4^{2-} Anion on Ethanol Electrooxidation at Decorated Platinum Electrode.

Most of the previous investigations on ethanol electrooxidation have been performed in strong acid or strong alkaline medium, while such a reaction in weak acid and neutral medium is much less studied in the reported literatures [53-54]. Therefore, when the acidity of the electrolyte is changed

from strong acid to neutral condition, the respective effect of both H^+ cation and SO_4^{2-} anion concentration on EOR should be desirable in order to understand the complex mechanisms of ethanol electrooxidation fully. Up to now, besides the strong acid medium is frequently adopted as supporting electrolyte for studying the mechanisms of EOR [55-58], the peculiar effect of SO_4^{2-} anions in the supporting electrolyte also attracts many researcher's attention [55, 57, 59-60]. To perceive the distinguishing characteristics regarding to the effect of H^+ cation on the EOR process, only when the sodium sulfate concentration added into the supporting electrolyte is fixed to 0.45 M, is it feasible to control the acidity of the electrolyte by solely increasing the sulfuric acid concentration.

As shown in Figure 5, there is the variation of cyclic voltammograms for 0.25 M ethanol oxidation in the electrolyte with different levels of acidity. Obviously, all of peak potentials in three surveillant voltammetric peaks of EOR shift more and more positive with the increasing concentration of sulfuric acid. However, the current of peak 1 and 2 during positive-going scan begin decrease from their maximum at H_2SO_4 concentration of approximately 1.0×10^{-3} M, while the ascending changes for the peak 4 are also observed when sulfuric acid concentration is continuously increased beyond 1.0×10^{-3} M. In addition, it is much extraordinary that the descending changes are also observed simultaneously for the peak 5.

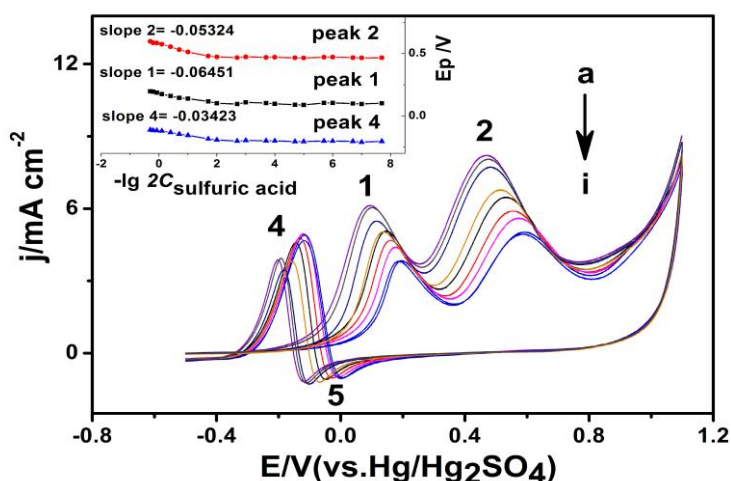


Figure 5. The effect of acidity on cyclic voltammograms of 0.25 M ethanol at Nd-Fe-Mo decorated electrode. Supporting electrolyte is composed of 0.45 M sodium sulfate + x M sulfuric acid. The serial curves are corresponding to different concentration of sulfuric acid: (a) 1.0×10^{-3} M, (b) 5.0×10^{-3} M, (c) 1.0×10^{-2} M, (d) 5.0×10^{-2} M, (e) 0.10 M, (f) 0.20 M, (g) 0.40 M, (h) 0.60 M and (i) 0.80 M, respectively. Inset curves show the relationship between the peak potentials and logarithm of sulfuric acid concentration.

Especially, the two forward peaks' current density decrease obviously, but the backward peaks' current density for peak 4 varies reversely with the increasing concentration of sulfuric acid. Razmi et al. also observed similar tendency for ethanol electrooxidation at H_2SO_4 concentrations ranging from 0.20 M to 1.0 M, and the maximum current density of the forward peaks 1 was merely achieved at 0.20 M H_2SO_4 [61].

On the other hand, the relationship between the three peaks' potentials and the logarithm of the sulfuric acid concentration exhibits a good linearity from 5.0×10^{-3} M to 1.0 M. If the pH value is approximatively calculated by H^+ concentration from only sulfuric acid contribution, the slope of Nernst relationship would reveal the information about a $-ne/-mH^+$ proton-coupled electrochemical reaction process [45]. In fact, the three linearly regressed equations are E_p (peak 1) = $0.1816 - 0.05324 \times \text{pH}$ ($r^2 = 0.9980$), E_p (peak 2) = $0.5776 - 0.06451 \times \text{pH}$ ($r^2 = 0.9962$) and E_p (peak 4) = $-0.1203 - 0.03423 \times \text{pH}$ ($r^2 = 0.9930$), respectively. The slopes in the equations obtained above clearly imply that the pathways of ethanol electrooxidation for both peak 1 and peak 2 have an equal number of deprotonation and electron transfer loss during the electrode reaction process, but the pathway of peak 4 has the feature of $-2ne/-nH^+$ process. Given this, it is inferred that when the sulfuric acid concentration increases above 1.0×10^{-3} M level, the inhibitory effect of H^+ plays a dominant role due to the deprotonation process which is the rate-limiting step of ethanol oxidation.

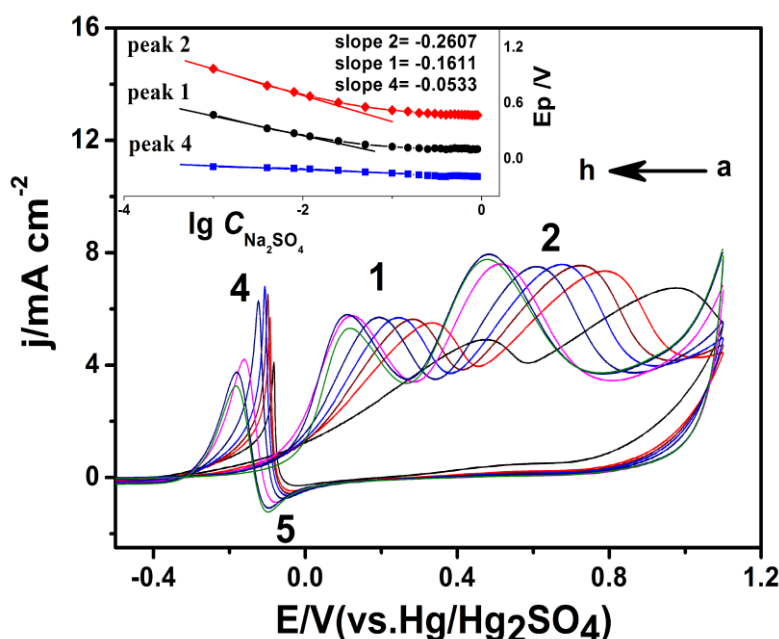


Figure 6. The effect of sodium sulfate concentration on cyclic voltammograms of 0.25 M ethanol at Nd-Fe-Mo decorated electrode. Supporting electrolyte is composed of x M sodium sulfate + 1.0×10^{-3} M sulfuric acid. The serial curves are corresponding to different concentration of sodium sulfuric: (a) 1.0×10^{-3} M, (b) 4.0×10^{-3} M, (c) 8.0×10^{-3} M, (d) 1.2×10^{-2} M, (e) 2.5×10^{-2} M, (f) 0.15 M, (g) 0.45 M and (h) 0.65 M, respectively. Inset curves show the relationship between peak potentials and the logarithm of sodium sulfate concentration.

Furthermore, the effect of SO_4^{2-} anions on the EOR is studied as well. Fixed the sulfuric acid at 1.0×10^{-3} M, the effect of SO_4^{2-} anions on the voltammetric peaks of ethanol oxidation in weak acidic medium can be immediately observed when the added amount of sodium sulfate is changed. As seen in Figure 6, the forward peak's current density of ethanol oxidation slightly increases with increasing concentration of sodium sulfate and arrives at the maximum in the electrolyte containing 0.45 M

Na₂SO₄, while the voltammetric profile of the backward peak 4 during reverse-going scan undergoes remarkable transformation from a steep curve to a plain profilogram.

Simultaneously, all peak potentials of ethanol oxidation steadily shift to negative potentials and finally reach a stable value. As shown in Figure 6 inset, the peak potential is in proportion to the logarithm of sodium sulfate concentration from 1.0×10^{-3} M to 0.025 M, and the regression equations are E_p (peak 1) = $-0.05924 - 0.1611 \times \lg C$ ($r^2 = 0.9974$), E_p (peak 2) = $0.1804 - 0.2607 \times \lg C$ ($r^2 = 0.9968$) and E_p (peak 4) = $-0.2079 - 0.05326 \times \lg C$ ($r^2 = 0.9981$), respectively. Consequently, it is suggested that although the increasing concentration of sodium sulfate in the supporting electrolyte can largely reduce impedance of electrolyte and leads to shift more negative values of the anodic peak potentials, the variational profilogram of peak 4 should prove the favorable effect of SO₄²⁻ anions on EOR and the existence of SO₄²⁻ anions even promotes the electrocatalytic oxidation reaction of ethanol at Nd-Fe-Mo decorated electrode in some sense. By combining with the results from Figure 5 and Figure 6, it is deduced that when acidity of the electrolyte is much high and the effect of Na⁺ cation is inferior to that of SO₄²⁻ anion, which have discussed extensively in the studies of the formic acid oxidation reaction on the same Nd-Fe-Mo decorated Pt electrode [46], the complication effect of pH and SO₄²⁻ anion to ethanol electrooxidation is mainly caused by the suppression of H⁺ rather than the benefit due to existence of SO₄²⁻ anion. Thus, the appropriate concentration of both sodium sulfate and sulfuric acid is selected to be 0.45 M and 1.0×10^{-3} M, respectively. Under the experimental condition, the electrooxidation behavior of ethanol in weak acidic medium is apparently superior to that in strongly acidic medium.

Kutz [57] and Méndez [62] reported that sulfate anions could co-adsorb with acetate as a surface-adsorbed oxidation intermediate of ethanol. In the present study, since the ordered adsorbent layer of (bi)sulfate anions was easily established on the Pt surface in low-concentration sodium sulfate solutions [63], the phenomena mentioned above might be due to the competitive adsorption of HSO₄⁻ /SO₄²⁻ anions on the decorated platinum surface by which some poisoning species such as CO_{ads} could be removed by an oxidative manner.

On the other hand, it was investigated by Ferreira et al. that the electrooxidation of ethanol on a smooth polycrystalline Pt electrode in the presence of different concentration of sulfuric acid. The authors reported that the maximum of the forward peak current density could be obtained in a 5.0×10^{-2} M sulfuric acid solution and the pathway of CO₂ formation was more strongly affected by the co-adsorption of sulfate anions than the formation of acetaldehyde and acetic acid [59]. Moreover, Basu et al. also observed that the DEFC performance was improved slightly with the proper increase in the ratio of sulfuric acid to ethanol in the electrolyte [60]. Thus, to my way of thinking, the effect of SO₄²⁻ anions on the EOR process might be more reasonably interpreted as helpful ion association with water molecular for the formation of Pt-OH in order to avail the surface dehydrogenation step of some intermediates in ethanol electrooxidation [2, 5, 9, 61].

3.3. Effect of Ethanol Concentration on Electrocatalytic Process of EOR.

To understand the effect of ethanol concentration on the electrocatalytic activity of decorated platinum surface, cyclic voltammetric experiments are performed at the ethanol concentrations in the

range of 0.010–3.00 M. As shown in Figure 7, five distinct current peaks including three forward peaks in positive-going sweep and two backward peaks in negative-going sweep are observed. Obviously, the magnitude of all peak currents in the voltammograms is correlated with the concentrations and each peak is associated with the distinct voltammetric behavior. For example, the profile of peak 3 merely starts to grow at ethanol concentration above 0.50 M. Moreover, it is noted that along with increasing the concentration of ethanol, the peak potentials of ethanol oxidation all slightly shifts to the positive values.

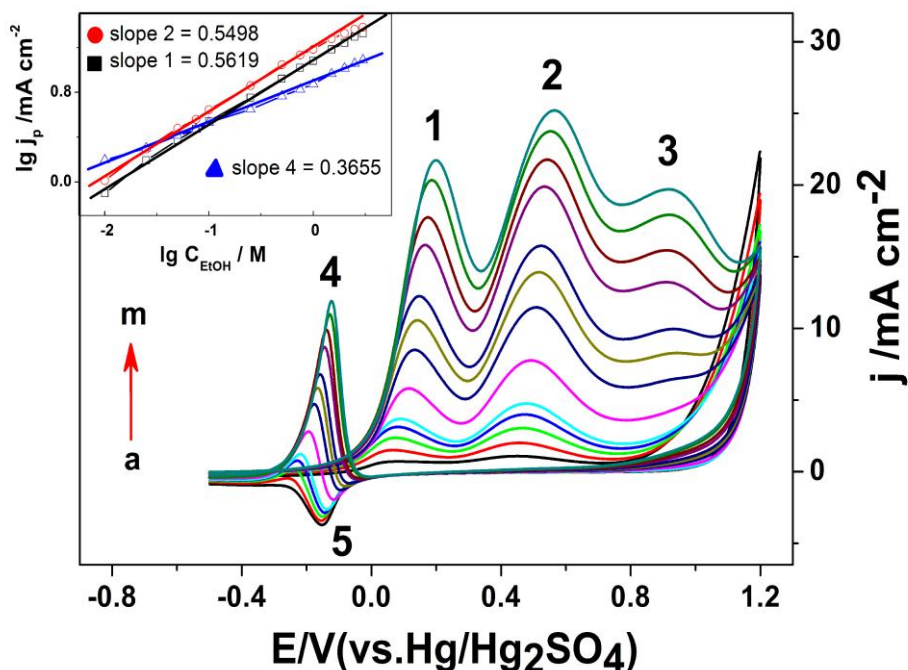


Figure 7. The cyclic voltammograms of ethanol oxidation at different ethanol concentration: (a) 0.010 M, (b) 0.025 M, (c) 0.050 M, (d) 0.075 M, (e) 0.10 M, (f) 0.25 M, (g) 0.50 M, (h) 0.75 M, (i) 1.00 M, (j) 1.50 M, (k) 2.00 M, (l) 2.50 M and (m) 3.00 M, respectively. Inset curves show the double logarithm graph between peak current and ethanol concentration.

However, it is also found that the current of the four peaks are distinctly enhanced, whereas that of peak 5 reduces and disappears finally. Interestingly, the moving direction of peak potential acts to oppose the potential scan direction for peak 4 and peak 5, which implies that oxidation process related to peak 4 could have some properties of autocatalytic oxidation.

In addition, a series of cyclic voltammetric experiments are performed on different decorated platinum electrodes with different geometrical areas. It is found that the absolute currents of two forward peaks for the EOR are proportionally enhanced with respect to the geometrical area of the decorated electrodes, while their peak current densities for the same ethanol concentration can be normalized to the identical values. This quantitative tendency suggests that there possibly exists a surface-sensitive electrochemical process corresponding to the overall ethanol oxidation. In other words, the enlargement of the anodic catalyst's total surface area can be a feasible scheme for improving the output power of DEFC systems [64].

However, the relationships between peak current density and ethanol concentration for each peak have some dissimilarity. The logarithmic values of peak current densities for peak 1, peak 2 and peak 4 are linear with the logarithmic curve of the ethanol concentration, but the peak current densities relating to peak 3 and peak 5 express a linear and a semi-logarithmic relationship to the concentration of ethanol, respectively. Then, the overall reaction orders (m), is estimated as 0.5619 for peak 1, 0.5498 for peak 2 and 0.3655 for peak 4 from the slopes of curves, respectively (see Figure 7 inset). And the obtained m values are approximately consistent with those reported in other studies [65-66]. Especially, the slopes in the double logarithmic curve between the peak current density and ethanol concentration for two forward oxidation peaks maintains the similar values that are less than an unit. These results indicate that the electrooxidation process corresponding to the two forward oxidation peaks of ethanol is coincided with the consecutive reaction model, in which the surface catalytic reaction on the initial oxidation stage of ethanol plays a key role [9, 65-66].

In the past years, there have been many investigations focusing on the effects of ethanol concentration related to the pathways of ethanol electrooxidation [66-69]. And it was found that the product contributions by producing CO_2 , acetic acid and acetaldehyde through the different pathways seems to depend on the ethanol concentration at the platinum surface [20]. The feature of peak 4 should be definitely explained to be the direct oxidation of ethanol by a special pathway but only a surface reactivation of some adsorptive species [69]. Significantly, in other reports, the reaction pathway forming CO_2 , which represents the production of a C-C bond cleavage, is not considered to have any benefit from increasing ethanol concentration [68]. Herein, since the high current density ratio $j_{\text{peak 1}}/j_{\text{peak 2}}$ corresponds to the increase in CO_2 production [70], the results in inset curves of Figure 7 would further indicate that the change of initial ethanol concentration in electrolytes does hardly favor the C1 pathway toward the formation of CO_2 in any concentration range, because of the negligible difference on the slopes between the double logarithmic curve relating to peak 1 and peak 2.

Moreover, two interesting phenomena should be noted. One is that the appearance current density of peak on the Nd-Fe-Mo polymer decorated platinum electrode is apparently superior to that on Rh/Pt bilayer decorated platinum electrode at same concentration of ethanol [29]. The other is salting-out effect of ethanol in the supporting electrolyte containing 0.45 M Na_2SO_4 . No sooner did the ethanol concentration in the electrolyte exceed 5.0 M than a white crystalline solid like-ice shape appeared; even the entire electrolyte liquid was coagulated to a solid state at lower temperature. The results are perhaps crucial to ascertain the maximal useable concentration of ethanol fuel in the saliferous electrolyte.

3.4. Effect of Potential Scan Rate on the Cyclic Voltammograms of Ethanol Oxidation.

Due to the relationship between the peak parameters and potential scan rate in the cyclic voltammograms, substantial kinetics information regarding to the electrocatalytic reaction should be gained [71]. Unfortunately, as seen in Figure 4 inset, the recording cyclic voltammograms that has achieved its stable voltammetric response are too time-consuming to study the electrochemical kinetics of the ethanol oxidation process on the bare platinum electrode. But the more accurate kinetics information can be expectably obtained with the Nd-Fe-Mo decorated electrode.

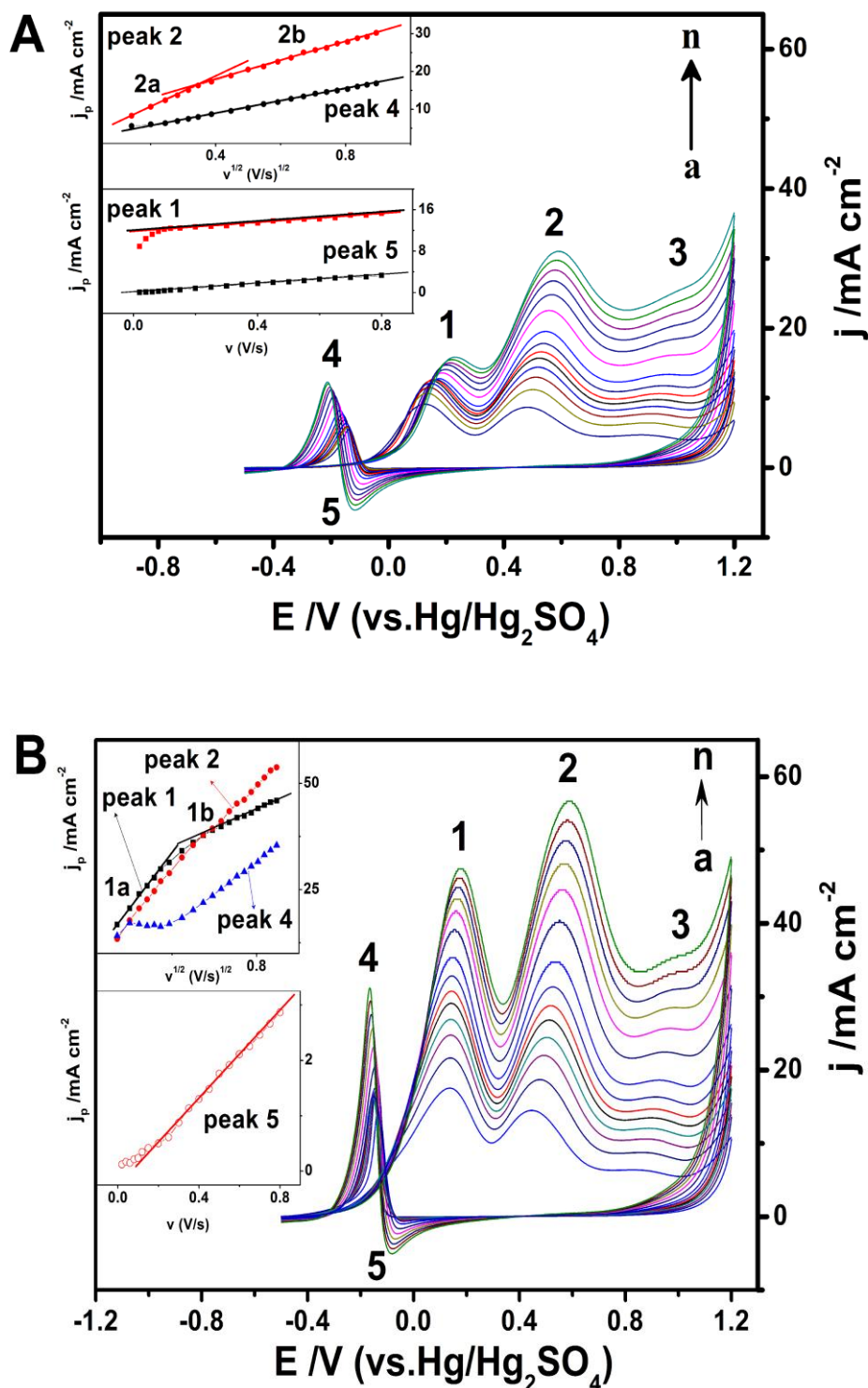


Figure 8. Cyclic voltammograms of 1.00 M ethanol oxidation on Nd-Fe-Mo decorated electrode at different temperature of (A) 25°C and (B) 45°C. The serial curves are corresponding with different scan rate (Vs^{-1}): (a) 20, (b) 40, (c) 60, (d) 80, (e) 100, (f) 120, (g) 150, (h) 200, (i) 300, (j) 400, (k) 500, (l) 600, (m) 700 and (n) 800, respectively.

As shown in Figure 8, five voltammetric peaks for 1.00 M ethanol oxidation on decorated platinum electrodes are distinctly perceived at different scan rates. Among the five current peaks, three

forward peaks and one backward peak are oxidative peaks and the other backward peak is a reductive peak. Firstly, considering the peak current variation, Figure 8A inset shows that peak current density of peak 1 and peak 5 is in proportion to scan rate in a certain range, but that of peak 2 and peak 4 is in proportion to the square root of the scan rate at 25°C (see Table.1).

Table. 1. Relationship between the peak permanent and scan rate corresponding to the cyclic voltammograms of 1.00 M ethanol electrooxidation

Peak number	^a Relationship of j_p vs v	
	25°C	45°C
Peak 1	$j_{p(1b)} = 11.7702 + 4.3169 \times v$ (n=14, $r^2=0.9963$)	$j_{p(1b)} = 24.8515 + 23.7843 \times v^{1/2}$ (n=10, $r^2=0.9985$)
Peak 2	$j_{p(2b)} = 7.6854 + 25.1917 \times v^{1/2}$ (n=15, $r^2=0.9990$)	$j_{p(2b)} = 11.2590 + 47.0438 \times v^{1/2}$ (n=10, $r^2=0.9984$)
Peak 4	$j_{p(4b)} = 2.9998 + 16.3995 \times v^{1/2}$ (n=18, $r^2=0.9996$)	$j_{p(4b)} = 1.0920 + 38.1531 \times v^{1/2}$ (n=12, $r^2=0.9996$)
Peak 5	$j_p = -0.02014 + 4.2619 \times v$ (n=20, $r^2=0.9986$)	$j_{p(4b)} = -0.3055 + 3.9857 \times v$ (n=12, $r^2=0.9984$)

^a All of data was extracted from Fig.8's voltammogram in the article and the regression equation between j_p and v was calculated from the total 20 data points in the scan range of 50-800 mVs⁻¹. The subscripts (*b*) of j_p expressed that some peak's equations were related to a few data points in the second piece of linear range of j_p vs. v curve at the higher scan rate.

Thus, although the voltammetric behavior of peak 1 and peak 2 is attributed to irreversible electrochemical processes, the electrochemical kinetic properties of the two anodic waves during the positive-going sweep are proven to exhibit different behavior at 25°C, which are a surface-controlled electrochemical process for peak 1 and a diffusion-controlled electrochemical process for peak 2. However, under the condition of 45°C, it is seen in Figure 8B that the current density of peak 1, peak 2 and peak 4 will have a piece of linear relationship between peak current density and the square root of the scan rate, while only the current density of peak 5 is still in proportion to the scan rate. Consequently, it needs to be noted why the rule of correspondence between peak current density and the scan rate for peak 1 seems far from the characters at different temperature. These results imply that the oxidative kinetics relating to peak 1 is enslaved to a homogeneous chemical reaction and/or to the CO stripping process, whereas the kinetic behavior of peak 2 and peak 4 is attributed to a normal diffusion-controlled electrochemical process without the influence from a homogeneous chemical reaction.

Furthermore, peak 3 also shows remarkable electrochemical behavior. With an increase in the scan rate, the profile of peak 3 gradually wears away, which do not keep coherence with other peaks. This feature suggests that peak 3 is related to the formation of some byproduct that is also affected by a homogeneous chemical reaction in abundant ethanol-containing bulk electrolyte. By studying the voltammetric behavior of a mixed electrolyte containing 0.25 M ethanol and 0.25 M ethyl acetate, it can be proven that although the ethyl acetate has poisoning effect to anodic catalysts, the formation of

peak 3 is not attributed to the oxidation of ethyl acetate. Since acetaldehyde is able to react with ethanol to form ethoxyhydroxyethane in aqueous solutions [58], in considering of the occurrence of peak 3's dependence on ethanol concentration, it is rationally ascribed that the electrooxidation current of peak 3 maybe come from ethoxyhydroxyethane oxidation, similar to the electrooxidation of a homologous compound such as dimethoxymethane in the high-potential region [72].

From another point of view, by comparing Figure 7 and Figure 8, it would be surprisingly discovered that when increasing the ethanol concentration, the peak 4 and peak 5 shift to more positive potentials; however, when increasing the scan rate, both of them shift to a negative potential. These results confirm that the oxidation currents of peak 4 and peak 5 are certainly related to the same active intermediate produced by the ethanol oxidation. However, up to now, the existence of peak 5 has been ignored in other reports, and its nature has remained completely unclear. Actually, from the viewpoint of electrochemistry, even though the peak potential of peak 5 is approximately -0.1 V (vs. Hg/Hg₂SO₄), which is near the reductive potential of PtO, the baffling voltammetric behavior of peak 5 cannot be satisfactorily explained by the simple fact that it is caused by only reduction of PtO. Huang and coworkers claimed that the linear and bridge-bonded forms of adsorbed CO were the only detectable reduction products from the reduction of CO₂ in the region of potentials at which there existed the adsorbed hydrogen [73]. Thus, in view of confirming feasibility of the mediated reduction of CO₂ on a Prussian blue-PAN modified electrode [74], it is more reasonable to partially ascribe peak 5 to the reductive reaction of CO₂ to explain the agreement with the voltammetric results described above. The remarkable appearance of peak 5 perhaps benefits from the multicomponent cooperation of the Nd-Fe-Mo cocatalyst.

Secondly, except for the information obtained from the peak currents, the variation of the peak potential regarding to the scan rate might provide much quantitative information for the electrochemical kinetics of ethanol oxidation. As seen in Figure 8B, when increasing the scan rate, the shape factor $E_p-E_{p/2}$ of peak 4 tends to be stable values (26 mV, 45°C). The oxidation process related to peak 4 can be estimated as a four-electron processes ($n_a=4.08$, 45°C), since the behavior of peak 4 could hypothetically correspond to the CV theory for the irreversible electron transfer processes and the theoretical value of $E_p-E_{p/2}$ equals to $50.9\text{mV}/0.48n_a$ [75]. Here, E_p and $E_{p/2}$ represent the peak potential and semi-peak potential, and n_a represents the electron transfer number of the rate-limiting step, respectively. Thus, if the two C-H bonds of ethanol molecular are simultaneously broken in dehydrogenation process, it can be understood that the results obtained above are reasonably consistent with a one-step concerted dehydrogenation mechanism of ethanol relating to a multi-electron transfer process, which is anticipated by the theoretical calculation for EOR process [76-77].

3.5. Effect of Temperature on the Electrocatalytic Process of Ethanol Oxidation.

The effect of temperature on the electrocatalytic process of 0.25 M ethanol oxidation is investigated from 25 to 75°C, as illustrated in Figure 9. It is noted that the current enhancement of peak 1 is superior to that of peak 2, while the peak potential of two oxidation waves correspondingly show some dissimilar movement. Surprisingly, the peak potential of peak 4 regularly moved to more positive potentials and its peak current also steadily increases with temperatures. Moreover, the

temperature coefficient of peak 4 is much close to that of peak 1 rather than to peak 2. The similar phenomena for ethanol oxidation were also observed on a carbon ceramic electrode modified with Pt particles by Razmi [61]. Furthermore, based on the linear relationships between $\ln j_p$ and $1/T$ at a high temperature range (Figure 9 inset curve), the apparent activation energies (E_a) are calculated by Arrhenius plots to be 22.78 kJ/mol for peak 1, 18.85 kJ/mol for peak 2 and 29.38 kJ/mol for peak 4, respectively. Interestingly, it is obvious that the apparent activation energies related to peak 1 is much closer to those value related to peak 2. And it can be deduced that the nature of peak 4 might be attributed to the formation of acetaldehyde in the EOR process because it possesses the highest E_a value among the three surveillant peaks, since the E_a values for CO_2 , acetic acid and acetaldehyde formation were reported to be 20, 28 and 43 kJ/mol, respectively [20]. As a result, the fact that the ratios $j_{\text{peak 1}}/j_{\text{peak 2}}$ increased by more than an unit may constitute an important criterion, which indicates the more complete oxidation of ethanol to carbon dioxide via the C1 pathway.

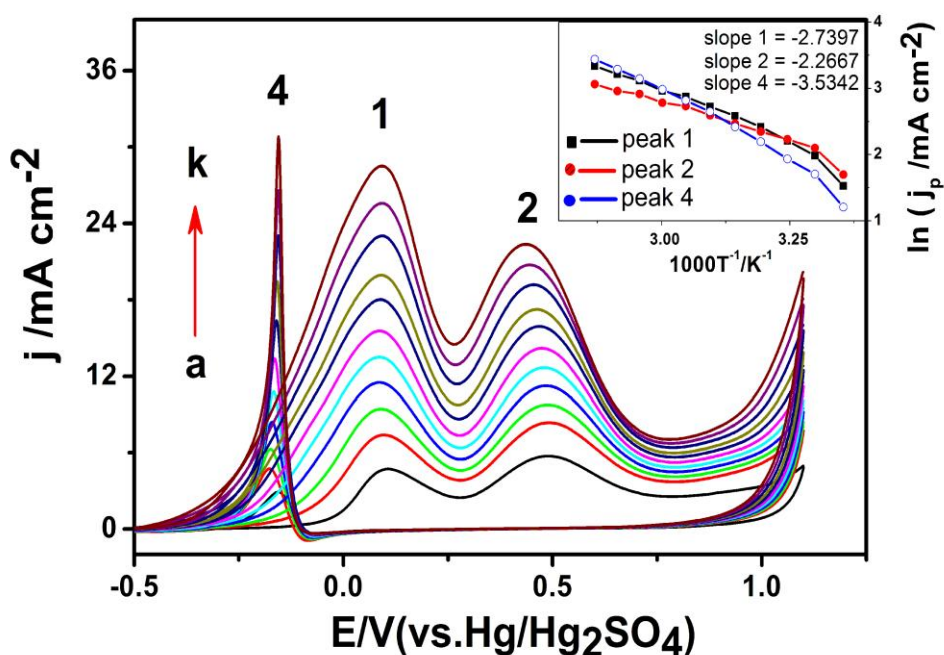


Figure 9. Cyclic voltammograms of 0.25 M ethanol oxidation on Nd-Fe-Mo decorated electrode at different temperature: 25°C (a), 30°C (b), 35°C (c), 40°C (d), 45°C (e), 50°C (f) 55°C (g) 60°C (h), 65°C (i), 70°C (j) and 75°C (k), respectively. Inset curves show Arrhenius plots of ethanol oxidation corresponding to peak 1, peak 2 and peak 4 in the cyclic voltammograms.

Herein, the Arrhenius plots corresponding to peak 1, peak 2 and peak 4 exhibits non-linear characters across the low temperature region. These behaviors imply that the oxidation process corresponding to three oxidative peaks might have some characters of the electrochemical kinetic wave. Subsequently, with increasing temperature, the peak potentials of peak 1 and peak 2 show an unusual shift and a shoulder-peak of peak 1 appear distinctly. Thus, it is inferred that the oxidation current of both peak 1 and peak 2 should not be caused by a single oxidizable species. Based on the present

experimental evidences, the peak 1 is attributed to the simultaneous oxidation of CO and ethanol while the peak 2 is attributed to the further oxidation of both acetaldehyde (AAL) and ethane-1,1-diol (ED) with Pt-OH as oxygen-supplying species, respectively [65, 79-80]. In the case of increasing temperature, the high value of $j_{\text{peak 1}}/j_{\text{peak 2}}$ implies that elevated temperature facilitates the more complete oxidation of ethanol to CO_2 [81-83]. Considering the recognizable mechanism of EOR that was previously outlined, the formation of acetaldehyde related to peak 4 via adsorption dehydrogenation of ethanol may be an important route for overall ethanol oxidation [9, 54, 58, 65-66].

3.6. Voltammetric Characteristics of Ethanol Oxidation during the Potentiostatic Electrolysis.

To evaluate the catalytic stability of ethanol oxidation on the Nd-Fe-Mo decorated electrodes, the steady-state potentiostatic electrolysis of ethanol is performed at different setting potentials. As seen in Figure 10A and 10B, when the controlled potentials in the chronoamperometric experiment are set at the optimized values, the chronoamperometric curves of EOR persisting 3600s of electrolysis can be conventionally obtained on both the bare platinum electrode and the Nd-Fe-Mo decorated electrode, respectively. At three concentration levels of ethanol (0.25 M, 0.50 M and 0.75 M), the steady-state current density of EOR averagely increase about 47% on the Nd-Fe-Mo decorated electrode compared with that on the bare platinum electrode, which is completely consistent with the results from cyclic voltammetry. Simultaneously, the dependence between the steady-state current of ethanol oxidation and different setting potentials after only electrolysis of 200s is illustrated in Figure 10C. With the experiment of potentiostatic electrolysis in such a short time, it is expected that the differences of steady-state current under different conditions would be certainly magnified in order to observe the voltammetric behaviors of the EOR more easily. As shown in the curve (a-c) of Figure 10C, the steady-state current peak in the curve (a) is observed at approximately 0.075 V and an unobvious shoulder-peak appears at 0.30 V. Obviously, with the increase of ethanol concentration, the maximum of applied potentials for steady-state electrolysis should slightly shift to more positive potentials. However, in contrast to the cyclic voltammograms of ethanol oxidation on the Nd-Fe-Mo decorated platinum electrode (Figure 10D), it is discovered that the potentials of 0.075V, which is corresponding to the maximum of steady-state currents in Figure 10C, is occurred slight before the potential of peak 1. And the potential of 0.30V, which is corresponding to the shoulder-peak currents in Figure 10C, is located at the concave between the potential of peak 1 and peak 2, respectively. The results about the potentiostatic electrolysis of ethanol seem to display inconsistent behavior with respect to its cyclic voltammetric characteristics. Namely, at the sloping portion of voltammetric curve before peak 1, the steady-state current of the EOR approaches its maximum, but in more positive potentials of peak 1, its steady-state current only exhibits a small shoulder-peak and sequentially declines. The results suggest that the poisoning species produced in the EOR process are mainly attributed to the formation of acetic acid, ethyl acetate and other products related to peak 2. In addition, another possible reason for the current decrease over the potential region of peak 2 may be due to the step-up potential mode. By employing this step-up mode, the formational condition of the unrecognized reactive intermediate will be completely restrained when applied potentials expand to more positive potentials, and will lead to vanishment of the steady-state current peak at approaching

the potential region of peak 2. Consequently, it is deduced that the course of ethanol electrooxidation can be greatly affected by the manner with which the potential is applied.

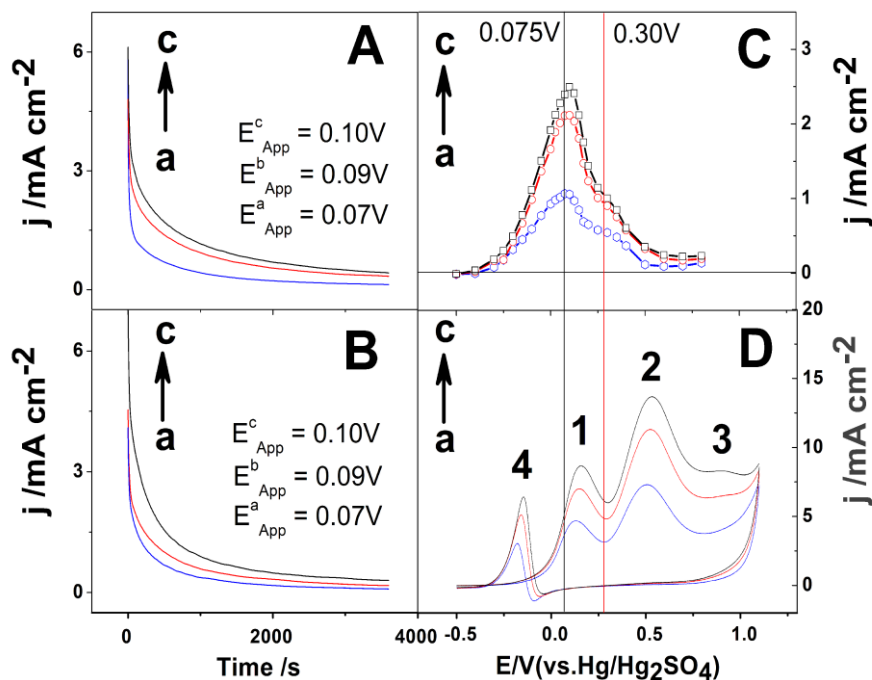


Figure 10. The relationship between steady-state current density of ethanol oxidation and setting potentials on both a Nd-Fe-Mo decorated platinum electrode (A) and a bare platinum electrode (B). Inset curves (C, D) show the applied potentials optimizing for steady-state electrolysis at 200s and a cyclic voltammograms of ethanol oxidation on the Nd-Fe-Mo decorated platinum electrode, respectively. Three concentration levels are of 0.25 M (a), 0.50 M (b) and 0.75 M (c).

On the other hand, the particular behavior of chronoamperometric curve for EOR within 200s is studied in detail. As shown in Figure 11, in the low potentials' region where only the electrooxidation reaction relating to peak 4 can take place, the chronoamperometric curves of ethanol will increase slightly up to maximum and then decrease sharply. With increase of the setting potentials from -0.30 V to 0.00 V, the time attaining to the maximum of steady-state current gradually shortened and the maximum profile of steady-state current curves disappears finally. It is noted that the abnormal kinetic behavior takes place within a narrow potential region. Thus, it provides direct evidence for the presence of an unrecognized reactive intermediate and for the autocatalytic characteristics of ethanol electrooxidation reaction over the low-potential region.

Moreover, when the setting potentials are varied from 0.10 V to 0.70 V, the steady-state current curve seems to intercrosses each other at some potential regions. As seen in Figure 11B, it is observe that there are three special potentials (-0.20 V, 0.075 V and 0.30 V), at which it corresponds to the appearance of abnormal kinetic behavior, the reachable maximum of steady-state current and the presence of a shoulder-peak of steady-state current, respectively. By comparing Figure 10 and 11, it can be comprehensible that during steady-state polarization, the steady-state current density ratio of

$j_{0.075\text{ V}}/j_{0.30\text{ V}}$ as similar to the peak current density ratio of $j_{\text{peak 1}}/j_{\text{peak 2}}$ in CV experiments can achieve to a high value. These results prove that the complete oxidation of fractional ethanol to carbon dioxide via 12 electrons per molecule carries out in the potential range of peak 1 [62].

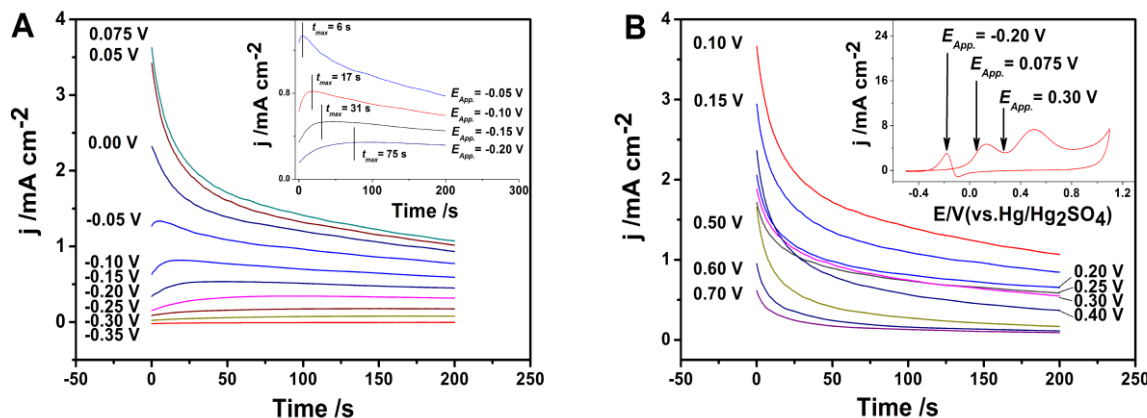


Figure 11. The dependence of potentiostatic electrolysis curves of 0.25M ethanol oxidation on the different setting potentials at the Nd-Fe-Mo decorated platinum electrode within 200s. Inset curves of Figure A and B show the kinetic behavior under the condition of steady-state electrolysis and a cyclic voltammograms of 0.25 M ethanol oxidation, respectively.

By means of the physicochemical techniques, Léger proved that although linearly adsorbed CO_{ads} is considered as a poisoning species in the EOR process, CO_{ads} may also act as a reactive intermediate [84]. Gomes also stated that in the case of the presence of ethanol on single crystal Pt electrode, both bridge and linearly bonded CO could be assuredly formed as the reaction intermediates and the maximum formation of bridge bonded carbon monoxide CO_{B} was achieved at ca. 0.40V (vs. RHE) [55,85]. What's more, Xia and coworkers reported that both bridge-bonded $(\text{CO}_{\text{B}})_{\text{ads}}$ and linear-bonded $(\text{CO}_{\text{L}})_{\text{ads}}$ could be formed just above 0.2 V (vs. RHE) at Pt(100) surface, and the interconversion between bridge and linearly bonded CO, turns out to be a common feature during the electrooxidation of small organic molecules in the low-overpotential region [86]. Thus, as discussed above, because the abnormal kinetic behavior related to the action of reactive intermediate will fade away when the applied potential goes into the region of distributive predominance for linearly bonded carbon monoxide CO_{L} , the unrecognized intermediate is reasonably assumed to be bridge-bonded carbon monoxide $(\text{CO}_{\text{B}})_{\text{ads}}$. Consequently, the puzzle arising from the inexplicable experimental evidences will be readily solved. If the promotive catalytic action of ethanol on Nd-Fe-Mo decorated electrode is partially attributed to the reactive intermediate $(\text{CO}_{\text{B}})_{\text{ads}}$, especially when using persisting electrolysis manner, the maximum Faradaic current density will be apt to produce more amounts of acetaldehyde and CO_2 in the range of low potentials.

Incidentally, though the poisoning to platinum electrodes for EOR process doesn't become aware easily in CV experiments, the reproducibility of gainable data in electrochemical experiments is often damaged by poisoning effects. Therefore, the good reproducibility in our experiment proves that

the new Nd-Fe-Mo decorated electrode exhibits better tolerance against toxic intermediate contamination, has excellent electrocatalytic stability, and will help to insight into the nature of EOR.

3.7. Interpretation of Voltammetric Peaks and Mechanism of Ethanol Oxidation.

To identify the reaction intermediates and elucidate the reaction mechanism of ethanol electrooxidation, various analytical techniques, such as differential electrochemical mass spectrometry (DEMS) [7, 14, 90], infrared spectroscopy (IRS) [54-55, 67, 69, 85-86, 88], chromatographic techniques [5-6], X-ray spectral analysis [78, 87], Raman spectroscopy [56] and vibrational sum-frequency generation spectroscopy (SFG) [57, 68] have been applied in this research field. By means of these methods, some details about the reaction mechanism of ethanol electrooxidation have been ascertained. In fact, because of the complexity of the EOR's mechanism and the limitations of each physicochemical methods applied in fuel cell research, the available experimental results can hardly explain the true mechanisms of EOR indisputably. Generally, the electrochemical techniques such as cyclic voltammetry and chronoamperometry, can supply more direct and accurate information to make the oxidation mechanism of ethanol comprehensibly. Therefore, in this paper, the possible mechanism model of ethanol electrooxidation is proposed by reasonable explanation of the five distinct current peaks of ethanol oxidation mentioned above.

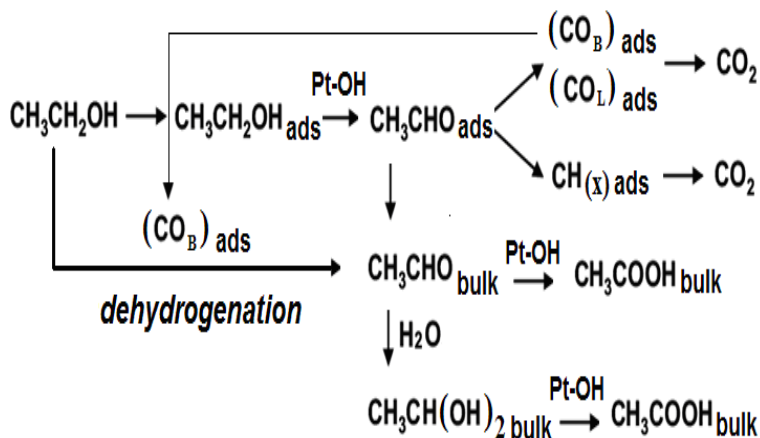
In the acidic solutions, the nature of the peak 1 has been extensively studied previously [53]. The proposed interpretation for this wave considers the peak current to be dependent of the formation of chemisorbed acetaldehyde (AAL) and Pt-OH. Because the peak potential for CO stripping usually overlaps with the peak 1's potential in the EOR and the mixture of CO₂ and acetaldehyde would be more likely to form in the same potentials region [88], the nature of peak 1 would be reasonably ascribed to ethanol electrooxidation to forming acetaldehyde and carbon dioxide with Pt-OH as oxygen-containing reactive intermediate. From this perspective, it is understandable why the electrochemical process related to peak 1 is a surface-controlled electrochemical process at 25°C, and then transfers to a diffusion-controlled electrochemical process at 45°C (cf. 3.4 section discussions above). Within the region of high potential, the nature of peak 2 and peak 3 is usually discussed much more questionably because it is subject to the stripping dissolution of some catalysts' compose. In this work, it is observed that the variational trend of peak 2 considerably depends on peak 1 in weak acidic medium. For example, the variations of peak 2 and peak 1 both exhibit a similar behavior due to the influence of SO₄²⁻ anions and H⁺ cation. However, the kinetics features of peak 2 seem to be a diffusion-controlled process without the conversion relating to the increase of temperature, which is different from that of peak 1. Thus, according to the discussion above, the nature of peak 2 is mainly attributed to further oxidation process of acetaldehyde (AAL) as a kind of intermedial product and ethane-1,1-diol (ED) as the hydrated compound of acetaldehyde in the supporting electrolyte. Furthermore, because the oxidation current of peak 3 increases obviously only at high ethanol concentrations and its relationship with scan rates exhibits an inconsequential variational trend, the nature of peak 3 is assumedly attributed to the electrooxidation of ethoxyhydroxyethane, whose existence has also been confirmed by liquid-state C¹³-NMR spectra during ethanol electrooxidation [58].

Except for the three forward oxidation peaks observed during positive-going sweep, the characteristics of the backward voltammetric peaks for the EOR during reverse-going sweep have bewildered researchers for a long time. In terms of the particular voltammetric behavior of peak 5 observed in the present work, the nature of peak 5 could be ascribed to the surface reduction of both PtO and some carbon dioxide due to the benefits from the multicomponent cooperation action of the Nd-Fe-Mo cocatalyst [73].

Comparatively, the nature of peak 4 is extremely significant. For instance, peak 4 is very susceptible to influences such as the amount of H^+ and SO_4^{2-} ions (see Figure 5 and 6), and its apparent activation energies is highest value among those in peak 1, peak 2 and peak 4 [20]. Willsau once stated that the unique product related to peak 4 is acetaldehyde rather than CO_2 , though they do so without presenting indisputable evidence [90]. Considering the fact that the potential of peak 4 is situated at a low overpotential of ca. -0.20 V, and the occurrence of peak 4 has much less contribution related to electrooxidation of intermediate product such as acetaldehyde by the assured CV experiments of 1.0 M acetaldehyde, the process associated with peak 4 is suggested to be the dehydrogenation of ethanol which is promoted by some reactive intermediates. In this work, all of inexplicable behaviors relating to peak 4 under the conditions of low potentials have been attributed reasonably to the assumption concerning adsorptive surface intermediates $(CO_B)_{ads}$, even though this definite results still need to be authenticated further by physicochemical methods on molecular level. With ATR-IR potentiodynamic spectra measurements, Heinen and co-workers observed that ethanol electrooxidation on a Pt electrode could lead to the formation of both linearly and multiply bound CO_{ads} , while the amount of CO_{ads} could be further increased during the second positive-going sweep with respect to that during the first positive-going sweep [55]. Based on the results supported with the actual evidences, the nature of peak 4 is primarily attributed to the more plentiful production of acetaldehyde via the diffusion-controlled dehydrogenation of ethanol at $(CO_B)_{ads}$ induced reaction point. Thus, the electrochemical nature relating to peak 4 is considered as the synergistic one-step dehydrogenation of ethanol to be induced by Pt- $(CO_B)_{ads}$ surface species ($n_a = 4.08$, $45^\circ C$). This notion in particular is consistent with the model describing a one-step concerted dehydrogenation pathway to produce acetaldehyde that is theoretically anticipated by applying periodic density functional theory for the EOR process on metal catalytic surfaces [76-77].

Currently, a generally accepted scheme of EOR on Pt-based catalysts is the dual pathway mechanism [2, 3, 9, 54, 57, 65, 69]. One pathway is the C1 pathway in which ethanol can be oxidized via $(CHO)_{ads}$ and CO_{ad} to CO_2 ; and the other is the C2 pathway via the oxidation of acetaldehyde (AAL) to acetic acid (AA). All acetaldehyde is derived from the dehydrogenation of ethanol. For each pathway, however, the PtOH produced from water dissociation provides a oxygen-containing reactive intermediate to accomplish both the oxidation of CO to CO_2 and AAL to AA [57, 80, 84]. Certainly, the production of acetaldehyde in the low-overpotential region helps to promote the transformational efficiency of C-C bond cleavage via the C1 pathway. Thus, it can be unambiguously explain why the C-C bond cleavage favors the low-overpotential region and why there is an inherent relationship between peak 1 and peak 4. To sum up, taking into account the rationality of the experimental conclusions, the possible electrooxidation mechanism of EOR in weak acidic medium is expressed as follows (see scheme 1).

According to the scheme1, because the voltammetric features of the EOR are quite similar to the voltammetric curve of primary alcohols with one to four carbon atoms in chain length on bright platinum electrodes [71, 89], the initial step of ethanol electrooxidation is attributed to the two dehydrogenation routes on the α -C atom of ethanol. One is traditional stepwise dehydrogenation



Scheme 1. Simplified representation of the possible mechanism for EOR process.

activated by PtOH, while the other is one-step concerted dehydrogenation pathway induced by $(\text{CO}_\text{B})_\text{ads}$, which have been theoretically anticipated by periodic density functional theory calculations. Hereafter, the further oxidation of acetaldehyde will act as the origination for the C1 pathway and C2 pathway double-path mechanism of ethanol oxidation. Conforming to the scheme 1 described above, it is reasonably explained by electrochemical experiment why the adsorbates on catalytic surface usually consists of C1 species, such as CO and CHO at potentials as low as 0.10 V and the C–C bond of an ethanol molecule can be easily broken at low potentials, which are observed by in situ SERS and SFG techniques [56-57].

4. CONCLUSIONS

In this work, the voltammetric behavior of ethanol electrocatalytic oxidation on an Nd-Fe-Mo decorated platinum electrode has been investigated by cyclic voltammetry and chronoamperometry. The synergistic catalytic effects of a decorated Nd-Fe-Mo material on polycrystalline platinum surface are excellently exhibited, and the oxidation peak current averagely increases 47% more than that on a bare polycrystalline platinum electrode. Based on the voltammetric characteristics of ethanol oxidation, the nature of five current peaks for EOR has been primarily explained. According to the experimental results, an unrecognized reactive intermediate is reasonably attributed to bridge-bonded carbon monoxide $(\text{CO}_\text{B})_\text{ads}$, and a new one-step concerted dehydrogenation model of EOR in weak acidic medium is proposed. As a result, it is inferred that the electrooxidation of ethanol mainly

follows different dehydrogenation pathways on the platinum electrode surface decorated with Nd-Fe-Mo deposits.

ACKNOWLEDGEMENTS

This work was financially supported by the Natural Science Foundation of China (U0734005, 20476108,) and the Natural Science Foundation of Gansu Province in China (096RJZA117).

References

1. J.M.Andújar, F.Segura, *Renewable and Sustainable Energy Reviews.*, 13 (2009) 2309.
2. C.Lamy, A.Lima, V.Lerhun, F.Delime, C. Coutanceau, J.-M. Léger, *J. Power Sources.*, 105 (2002) 283.
3. S.Q.Song, P.Tsiakaras, *Appl.Catal.B: Environ.*, 63 (2006) 187.
4. U.B.Demirci, *J. Power Sources.*, 169 (2007) 239.
5. S.Rousseau, C. Coutanceau, C.Lamy, J.-M. Léger, *J. Power Sources.*, 158 (2006) 18.
6. D.D.James, D.V. Bennett, G.C.Li, A.Ghumman, R.J. Helleur, P.G. Pickup, *Electrochem. Commun.*, 11 (2009) 1877.
7. L.Colmenares, H.Wang, Z.Jusys, L.Jiang, S.Yan, G.Q.Sun, R.J. Behm, *Electrochim. Acta.*, 52 (2006) 221.
8. G.Andreadis, V.Stergiopoulos, S.Song, P.Tsiakaras, *Appl.Catal.B: Environ.*, 100 (2010) 157.
9. F.Vigier, S.Rousseau, C.Coutanceau, J.-M. Léger, C. Lamy, *Top. Catal.*, 40 (2006) 111.
10. E.Antolini, *Appl. Catal. B: Environ.*, 74 (2007) 337.
11. E.Antolini, *J. Power Sources.*, 170 (2007) 1
12. A.C.Chen, P. Holt-Hindle, *Chem. Rev.*, 110 (2010) 3767.
13. E.Antolini, E.R.Gonzalez, *Catal. Today.*, 160 (2011) 28.
14. J.P.I.de Souza, S.L. Queiroz, K.Bergamaski, E.R.Gonzalez, F.C.Nart, *J. Phys. Chem. B*, 106 (2002) 9825.
15. B.Liu, J.H. Chen, X.X. Zhong, K.Z.Cui, H.H.Zhou, Y.F.Kuang, *J. Colloid Interface Sci.*, 307 (2007) 139.
16. H. B. Suffredini, G. R.Salazar-Banda,; L. A. Avaca, *J.Power Sources.*, 171 (2007) 355.
17. H.L.Pang, J.H.Chen, L.Yang, B. Liu, X.X. Zhong, X.G. Wei, *J.Solid State Electrochem.* 12 (2008) 237.
18. E.Antolini, E.R. Gonzalez, *Solid State Ionics.*, 180 (2009) 746.
19. W.J.Zhou, Z.H. Zhou, S.Q. Song, W.Z. Li, G.Q.Sun, P. Tsiakaras, Q. Xin, *Appl. Catal. B: Environ.*, 46 (2003) 273.
20. H.Wang, Z.Jusys, R.J. Behm, *J.Phys.Chem.B*, 108 (2004) 19413.
21. C.Coutanceau, S.Brimaud, C.Lamy, J.-M. Léger, L.Dubau, S.Rousseau, F.Vigier, *Electrochim. Acta.*, 53 (2008) 6865.
22. L.Jiang, L.Colmenares, Z. Jusys, G.Q. Sun, R.J.Behm, *Electrochim. Acta.* 53 (2007) 377.
23. J.Ribeiro, D. M. dos Anjos, J.-M. Léger, F. Hahn, P. Olivi, A. R. de Andrade, G. Tremiliosi-Filho, K.B.Kokoh, *J.Appl.Electrochem.*, 38 (2008) 653.
24. N.Fujiwara, K.A.Friedrich, U.Stimming, *J. Electroanal. Chem.*, 472 (1999) 120.
25. G.A.Camara, R.B.de Lima, T. Iwasita, *J. Electroanal. Chem.*, 585 (2005) 128.
26. J. S.Spendelow, A.Wieckowski, *Phys.Chem.Chem.Phys.*, 6 (2004) 5094.
27. F.C.Simões, D.M.dos Anjos, F.Vigier, J.-M.Léger, F.Hahn, C.Coutanceau, E.R.Gonzalez, G.Tremiliosi-Filho, A.R.de Andrade, P.Olivi, K.B. Kokoh, *J.Power Sources.* 167 (2007) 1.
28. A.A.Abd-El-Latif, E.Mostafa, S.Huxter, G.Attard, H.Baltruschat, *Electrochimica Acta.*, 55 (2010) 7951.

29. R.T.S.Oliveira, M.C.Santos, B.G.Marcussi, S.T.Tanimoto, L.O.S.Bulhões, E.C.Pereira, *J.Power Sources.*, 157 (2006) 212.
30. V.P.Santos, V.D. Colle, R.B.de Lima, G. Tremiliosi-Filho, *Electrochim. Acta.*, 52 (2007) 2376.
31. Y.X.Bai, J.J.Wu, X.P.Qiu, J.Y.Xi, J.S.Wang, J.F. Li, W.T.Zhu, L.Q.Chen, *Appl. Catal. B: Environ.*, 73 (2007) 144.
32. A. O.Neto, M. Linardi, D.M.dos Anjos, G.Tremiliosi-Filho, E.V.Spinacé, *J.Appl.Electrochem.*, 39 (2009) 1153.
33. R. M. S.Rodrigues, M. M.Tusi, M. H.Chikasawa, C.A.L.G.O.Forbicini, M.Linardi, E.V.Spinacé, A.O.Neto, *Ionics.*, 17 (2011) 189.
34. J. M.Anderson, J.Patel, A. S Karakoti, N. Greeneltch, D. J. Díaz, S. Seal, *Electrochim. Acta.* 56 (2011) 2541.
35. J. H.Zhou, J. P.He, T.Wang, X.Chen, D.Sun, *Electrochim. Acta.*,54 (2009) 3103.
36. N. R. de Tacconi, K.Rajeshwar, R. O. Lezna, *Chem. Mater.*,15 (2003) 3046.
37. G.Selvarani, S.K.Prashant, A.K.Sahu, P.Sridhar, S.Pitchumani, A.K.Shukla, *J.Power Sources.*, 178 (2008) 86.
38. M.Jayalakshmi, F.Scholz, *J.Power Sources.*, 91 (2000) 217.
39. M.H.Pournaghi-Azar, B.Habibi, *J. Electroanal. Chem.*, 605 (2007) 136.
40. T.R.I.Cataldi, D. Centonze, A.Guerrieri, *Anal. Chem.*, 67 (1995) 101.
41. S.Tanase, J. Reedijk, *Coord. Chem. Rev.*, 250 (2006) 2501.
42. R.Koner, M.G.B. Drew, A.Figuerola, C. Diaz, S.Mohanta, *Inorg. Chim. Acta.*, 358 (2005) 3041.
43. E.Chelebaeva, Y.Guari, J.Larionova, A.Trifonov, C. Guérin, *Chem. Mater.*, 20 (2008) 1367.
44. M.Yamada, S.Yonekura, *J.Phys.Chem.C*, 113 (2009) 21531.
45. Y. J. Ma, Y. Y.Pan, W. F.Wang, M. X.Yang, M. Zhou, *Chin. Chem. Lett.*, 21 (2010) 337.
46. Y. J. Ma, M. X.Yang, W. F.Wang, M. Zhou, J.Liu, T.T. Li, H. Chen, *Acta Chim. Sinica.*, 69 (2011) 262.
47. Q.L.Sheng, H.Yu, J.B.Zheng, *Electrochim. Acta.*, 52 (2007) 4506.
48. S.J.Dong, Z.Jin, *J. Electroanal. Chem.*, 256 (1988) 193.
49. V. M. Schmidt, R.Ianniello, E.Pastor, S.González, *J. Phys. Chem.*, 100 (1996) 17901.
50. X.Y. Wang, Y.Yukawa, Y.Masuda, *J. Alloys Compd.*, 290 (1999) 85.
51. S. Q. Liu, H.Y.Chen, *J. Electroanal. Chem.*, 528 (2002) 190.
52. X.L.Wu, M. H. Cao, C.W. Hu, X.Y. He, *Cryst.Growth Des.*, 6 (2006) 26.
53. K.D. Snell, A.G. Keenan, *Electrochim. Acta.*, 27 (1982) 1683.
54. S.C.S. Lai, S.E.F.Kleijn, F.T.Z. Öztürk, V.C.van Rees Vellinga, J. Koning, P. Rodriguez, M.T.M. Koper, *Catal. Today.*, 154 (2010) 92.
55. M. Heinen, Z. Jusys, R.J. Behm, *J. Phys. Chem. C.*, 114 (2010) 9850.
56. S.C.S. Lai, S.E.F. Kleyn, V. Rosca, M.T.M. Koper, *J. Phys. Chem. C.*, 112 (2008) 19080.
57. R.B. Kutz, B.Braunschweig, P.Mukherjee, R.L.Behrens, D.D.Dlott, A.Wieckowski, *J. Catal.*, 278 (2011) 181.
58. I. Kim, O.H. Han, S.A. Chae, Y. Paik, S.H. Kwon, K.S. Lee, Y.E. Sung, H. Kim, *Angew.Chem. Int. Ed.*,50 (2011) 2270.
59. R.S. Ferreira Jr., V.R.Oliveira, R.G.C.S. Reis, G.Maia, G.A.Camara, *J. Power Sources.*, 185 (2008) 853.
60. S. Basu, A. Agarwal, H. Pramanik, *Electrochem. Commun.*, 10 (2008) 1254.
61. H. Razmi, E.Habibi, H. Heidari, *Electrochim. Acta.*, 53 (2008) 8178.
62. E.Méndez, J. L.Rodríguez, M. C. Arévalo, E.Pastor, *Langmuir*, 18 (2002) 763.
63. B. Braunschweig, P. Mukherjee, D.D. Dlott, A. Wieckowski, *J. Am. Chem. Soc.* 132 (2010) 14036.
64. M.H.Chen, Y.X. Jiang, S.R.Chen, R. Huang, J. L.Lin, S.P.Chen, S.G. Sun, *J. Phys.Chem. C*, 114 (2010) 19055.
65. H. Hitmi, E.M. Belgsir, J.-M. Léger, C. Lamy, R.O. Lezna, *Electrochim, Acta.*, 39 (1994) 407.

66. J. Otomo, S. Nishida, H. Takahashi, H. Nagamoto, *J. Electroanal. Chem.*, 615 (2008) 84.
67. G. A. Camara, T. Iwasita, *J. Electroanal. Chem.*, 578 (2005) 315.
68. J. F. Gomes, B. Busson, A. Tadjeddine, *J. Phys. Chem. B*, 110 (2006) 5508.
69. M. J. Giz, G.A. Camara, *J. Electroanal. Chem.* 625 (2009) 117.
70. E.P. Leão, M.J. Giz, G.A. Camara, G. Maia, *Electrochim. Acta.*, 56 (2011) 1337.
71. C.G. Lee, M. Umeda, I. Uchida, *J. Power Sources.*, 160 (2006) 78.
72. Z.Y. Zhou, D.J. Chen, H. Li, Q. Wang, S.G. Sun, *J. Phys. Chem. C*, 112 (2008) 19012.
73. H. Huang, C. Fierro, D. Scherson, E. B. Yeager, *Langmuir*, 7 (1991) 1154.
74. M. Nakayama, M. Iino, K. Ogura, *J. Electroanal. Chem.*, 440 (1997) 251.
75. R. Sousa Jr., D. M. dos Anjos, G. Tremiliosi-Filho, E.R. Gonzalez, C. Coutanceau, E. Sibert, J.-M. Léger, K. B. Kokoh, *J. Power Sources.*, 180 (2008) 283.
76. M. Li, W.Y. Guo, R.B. Jiang, L.M. Zhao, X.Q. Lu, H.Y. Zhu, D.L. Fu, H.H. Shan, *J. Phys. Chem. C*, 114 (2010) 21493.
77. H.F. Wang, Z.P. Liu, *J. Phys. Chem. C*, 111 (2007) 12157.
78. I. G. Casella, E. Desimoni, *Electroanalysis*, 8 (1996) 447.
79. B. Rasch, T. Iwasita, *Electrochim. Acta.*, 35 (1990) 989.
80. M.J.S. Farias, G.A. Camara, A.A. Tanaka, T. Iwasita, *J. Electroanal. Chem.*, 600 (2007) 236.
81. S. Sun, M.C. Halseid, M. Heinen, Z. Jusys, R.J. Behm, *J. Power Sources.*, 190 (2009) 2.
82. S. Q. Song, Y. Wang, P.K. Shen, *Chin. J. Catal.*, 28 (2007) 752.
83. J. Mann, N. Yao, A. B. Bocarsly, *Langmuir*, 22 (2006) 10432.
84. J.-M. Léger, S. Rousseau, C. Coutanceau, F. Hahn, C. Lamy, *Electrochim. Acta.*, 50 (2005) 5118.
85. J.F. Gomes, B. Busson, A. Tadjeddine, G. Tremiliosi-Filho, *Electrochim. Acta.*, 53 (2008) 6899.
86. X. H. Xia, H.-D. Liess, T. Iwasita, *J. Electroanal. Chem.*, 437 (1997) 233.
87. J. Melke, A. Schoekel, D. Dixon, C. Cremers, D. E. Ramaker, C. Roth, *J. Phys. Chem. C*, 114 (2010) 5914.
88. M.H. Shao, R.R. Adzic, *Electrochim. Acta.*, 50 (2005) 2415.
89. P. Katikawong, T. Ratana, W. Veerasai, *J. Chem. Sci.*, 121 (2009) 329.
90. J. Willsau, J. Heitbaum, *J. Electroanal. Chem.*, 194 (1985) 27.